ANNALS OF GEOPHYSICS, 68, 1, V110, 2025; doi:10.4401/ag-9172
OPEN ACCESS

# Scenario impact assessment for volcanoes using the OpenQuake engine

Catalina Yepes-Estrada[*,1], Anirudh Rao[1], Julián Andrés Ceballos[2], Susanna Jenkins[3], Marco Pagani[1], Vitor Silva[1], Luis Gerónimo Valencia Ramírez[2], Carlos Laverde[2], Miguel Mora[2]

(1) Global Earthquake Model (GEM) Foundation, Pavia, Italy
(2) Colombian Geological Survey (SGC), Bogota, Colombia
(3) Earth Observatory of Singapore, Asian School of the Environment, Nanyang Technological University (NTU), Singapore

Article history: received September 30, 2024; accepted February 26, 2025

## Abstract

This study introduces a unified framework for evaluating the physical impacts of earthquakes and volcanic eruptions on buildings, leveraging upon the existing capabilities of the OpenQuake engine for earthquake risk assessment and various existing packages for computing volcanic hazard footprints. We illustrate the capabilities of the new OpenQuake volcanic scenario module using two case studies: a VEI (Volcanic Explosivity Index) 3-4 eruption of Nevado del Ruiz volcano in Colombia and a VEI 6 eruption of Mount Pinatubo in the Philippines, employing various methods for simulating hazard footprints for tephra fall, lava flows, pyroclastic density currents, and lahars. The findings demonstrate the versatility of OpenQuake in managing diverse geohazards and its potential for further extension to other hazards, while this integration advances our ability to assess and manage disaster risk.

Keywords: Volcanic risk scenario; Risk assessment; Disaster risk reduction; OpenQuake

## 1. Introduction

The Ring of Fire is responsible for about 90% of the global seismic activity and includes 75% of the world's active volcanoes. According to the Global Assessment Report (GAR, 2015) by the United Nations Office for Disaster Risk Reduction (UNDRR), earthquakes and volcanic eruptions are responsible for 80% of the average annual economic losses in many Pacific countries. Over the past 250 years, volcanic eruptions from just six volcanoes have resulted in nearly 160 thousand fatalities (Brown et al., 2017). Notably, the 1985 Nevado del Ruiz eruption in Colombia and the 1883 Krakatau eruption in Indonesia alone were responsible for approximately 24,000 and 36,000 fatalities respectively, pointing to the potential for devastating mass casualties in a single event. Volcanoes are responsible for more than half of Indonesia's average annual economic losses, and almost 10% of the losses in the Philippines and Papua New Guinea. Over the past 12-years, earthquakes have caused more than 2.4 million fatalities, displaced nearly 25.4 million people and generated economic losses exceeding $976 billion, representing almost 70% of the reconstruction cost across all natural hazards-related disasters (EM-DAT, 2024). High-casualty events such as the

2010 Mw 7.0 Haiti earthquake and the 1976 Mw 7.5 Tangshan earthquake in China show how single devastating events can cause nearly a quarter million deaths.

Risk assessment represents the first step to managing and mitigating future disaster risk. The UNDRR defines risk from natural hazards as "the potential loss of life, injury, or destroyed or damaged assets which could occur to a system, society or a community in a specific period of time, determined probabilistically as a function of hazard, exposure, vulnerability and capacity"[1]. The assessment of volcanic risks is a complex process. Volcanoes are geological systems capable of generating numerous, sometimes coincident, and often deadly hazardous natural phenomena (Martí Molist, 2017; Loughlin et al. 2015). These include lava flows, tephra fallout, lahars, pyroclastic density currents, debris avalanches, as well as fire, landslides, and tsunami hazards, which may interact and cascade over different temporal and spatial scales. Adding to this complexity are the dynamic characteristics of exposure and vulnerability, influenced by evolving human and environmental factors, which further challenge effective volcanic risk assessment.

In recent decades, significant progress has been made in improving volcanic hazard methodologies and modelling tools, particularly in the treatment of uncertainty (e.g. Marzocchi et al., 2021). On the other hand, volcanic risk assessment has gained increasing attention in recent years, as understanding the potential impacts of eruptions is critical for mitigating their effects on communities and infrastructure. Volcano observatories play a fundamental role in this process by monitoring volcanic activity, providing early warnings, and generating hazard and risk models that inform decision makers. Numerous studies have been conducted for volcanic risk assessment (e.g. Pomonis et al., 1999; Alberico et al., 2011; Jenkins et al., 2015; Spence et al., 2005; Wild et al., 2020; Bonadonna et al., 2021; Reyes-Hardy et al., 2024) using qualitative, semi-quantitative, or quantitative approaches. Loughlin et al. (2015) and Bonadonna et al. (2021) provide relevant examples of quantitative risk assessments focusing on specific volcanic hazards (e.g. tephra fallout and lava flows), as well as studies incorporating multiple volcanic hazards. However, comprehensive and multidisciplinary methods for evaluating vulnerability and assessing volcanic risk are still evolving, and no clear and common consensus has emerged (Bonadonna et al., 2018). Deligne et al. (2022) provide a review of advancements made over the past 20 years in characterizing the impacts of volcanic eruptions on the built environment.

The CRAVE project[2] (Collaborative Risk Assessment for Volcanoes and Earthquakes) – supported by the United States Agency for International Development (USAID) – was the opportunity to explore commonalities and capabilities in the volcano and earthquake fields. The Global Earthquake Model (GEM) Foundation and the Global Volcano Model (GVM) network led the project and received contributions from the Colombian Geological Survey (SGC), British Geological Survey (BGS), Earth Observatory of Singapore (EOS), University of Edinburgh, Volcano Disaster Assistance Program (VDAP) of the United States Geological Survey (USGS), Philippine Institute of Volcanology and Seismology (PHIVOLCS), and Badan Geologi (Indonesia). The project aimed to develop a common framework for assessing the impact of earthquakes and volcanoes on buildings and infrastructure, including the implementation of volcanic scenario in the OpenQuake engine, an open-source software (Pagani et al., 2014, and Silva et al., 2014) widely used by scientists and governmental institutions for national seismic hazard and risk assessments, such as Australia (Allen et al., 2018), Canada (Kolaj et al., 2023; Hobbs et al., 2023), New Zealand (Gerstenberger et al., 2024), Colombia (Arcila et al., 2020), Ecuador (Beauval et al., 2018), El Salvador (Lopez et al., 2024), Indonesia (Irsyam et al., 2020), Italy (Meletti et al., 2021), Taiwan (Chan et al., 2020).

The proposed framework was applied to three volcanoes in the Metropolitan District of Quito, DMQ, Ecuador. In collaboration with the Municipality of Quito (Metropolitan Directorate of Risk Management), Calderón et al. (2022) used a block-level building exposure model to evaluate volcanic scenarios, considering lahars in the Cotopaxí Eruption of 1877; lahars in the Guagua Pichincha Eruption from the X century; and tephra fall, and pyroclastic density currents in the Atacazo Ninahuilca Eruption of 5.440 to AP (N4). The models and results are openly available in the repository https://github.com/gem/treq-riesgo-urbano/tree/main/Quito/. One-page infographics were generated for each volcano, aimed at effectively communicating volcanic risk assessment results to stakeholders and the public. The infographics were carefully designed to convey the potential impacts of historical eruptions on the built environment, enhance societal risk awareness, and provide essential metrics to inform preparedness and response strategies.

1 https://www.undrr.org/terminology/disaster-risk.

2 https://www.globalquakemodel.org/proj/crave.

The following sections present the proposed framework for evaluating the physical impacts of volcanic eruptions on buildings and affected population, leveraging upon the OpenQuake engine and existing tools to generate the hazard footprint of the volcanic phenomena. By building on the existing capabilities of the OpenQuake engine for earthquake risk assessment, this work expands its functionality to also encompass volcanic hazards, in this case for tephra fall, lava flows, pyroclastic density currents, and lahars.

## 2. Volcanic risk scenario implementation in the OpenQuake engine

To evaluate and manage volcanic risk, it is crucial to identify how an active volcano (or volcanic system) has behaved in the past to infer future behaviour (Martí Molist, 2017). Not all hazards might be generated in every eruption and all volcanoes do not produce the same hazards. Volcanic eruptions can be characterized by the magnitude, intensity, duration, and associated eruptive phenomena. This information can be used to create eruption scenarios and related hazard maps, which constitute the basis of volcanic risk estimations and mitigation programs. The set of eruptive phenomena, which can be defined as the areas affected or impacted by each hazardous process, are called "hazard footprints".

The implementation of the volcanic risk scenario calculator in the OpenQuake engine uses the existing OpenQuake risk library[3], initially designed for earthquake risk assessment and loss estimation, and has since been expanded to support volcanic risk scenarios. This implementation builds upon existing tools to generate hazard footprints for four distinct volcanic hazards: tephra fall, lava flows, pyroclastic density currents, and lahars. These hazards can be modeled simultaneously, although they are treated independently, meaning that the impact of one hazard does not influence the others.

These hazard footprints can be derived either deterministically (from a single simulation) or probabilistically, where multiple simulations reflect the variability of the volcanic event under different assumptions. In the current implementation, hazard intensity is described quantitatively, such as tephra load in kilopascals (kPa) for tephra fall, while for lava flows, pyroclastic density currents, and lahars, hazard intensity is modelled as a binary phenomenon: "1" for affected areas and "0" for unaffected areas. While binary damage assumptions may oversimplify the complexity of real-world impacts (e.g. Meredith et al., 2022; Baxter et al., 2005; Jenkins et al., 2015b), this initial approach was adopted due to the limited availability of fragility models that relate continuous intensity measures to specific building classes. However, expanding the current framework to include continuous intensity measures alongside their corresponding fragility models is straightforward and remains a key focus for future improvements.

### 2.1 Methodology

The volcanic scenario implementation in the OpenQuake engine allows users to compute scenario-based building damage and consequence calculations for one or multiple types of volcanic hazards represented as a set of footprints (i.e., grids describing the spatial distribution of the intensity of a hazard parameter, e.g. thickness of the tephra fall produced by one eruption event). The implementation includes a scenario damage calculator and a scenario risk calculator.

The scenario damage calculator computes, for each volcanic hazard footprint, damage distribution statistics for each asset (i.e. buildings specified in the exposure model). For binary hazards, damage is either considered total or absent. In the case of tephra fall, however, the fragility model determines the probability of a building class exceeding a certain damage state for a given hazard intensity. The results include detailed damage statistics for each individual asset, aggregated damage data for each building class, and overall damage distribution across the region. Additionally, maps can be generated to visualize the spatial distribution of damaged buildings by number or area, providing an overview of the impacts within the region of interest. In addition, for tephra fall, users can include a "humidity amplification factor", which multiplies the hazard intensity (ash load) to account for humid conditions. The model generates outputs for both dry and wet conditions, reflecting the respective impacts of varying moisture levels on the ash load.

3 https://github.com/gem/oq-engine/tree/master/openquake/risklib.

A consequence model can be optionally included in addition to fragility models when estimating scenario damage under tephra fall. This model allows to estimate consequences, such as economic losses, fatalities or injuries, based on the calculated damage distribution. A consequence model defines a set of functions, describing the distribution of the loss (or consequence) ratio conditional on the damage states. These consequence functions can be currently defined in the OpenQuake engine by specifying the parameters of the continuous distribution of the loss ratio for each damage state specified in the fragility model for the corresponding loss type, and for each building typology present in the exposure model.

The scenario risk calculator functions similarly to the scenario damage calculator, but instead of using fragility models that predict damage states, it uses vulnerability models that define a mean loss ratio for each level of hazard intensity. Multiple loss types are supported, such as economic losses, downtime, area of buildings lost, occupant fatalities, and displaced population, among others. Scenario risk results are similar to the ones obtained with the scenario damage calculator, when fragility and consequence models are used. Since the case studies presented in this manuscript only explored damage impact without considering consequence models, Section 2.4 only focuses on fragility functions.

Figure 1 outlines the essential input models for conducting volcanic risk scenario calculations, including hazard footprints, exposure data, and vulnerability models. Hazard footprints can represent up to four simultaneous volcanic hazards. Exposure data, such as buildings and their occupants, can include various details at different geographical resolutions, as further elaborated in Section 2.3. The vulnerability model, applicable only to non-binary hazard intensities (i.e. tephra fall), can utilize either fragility and consequence models or vulnerability models, depending on the selected calculator.

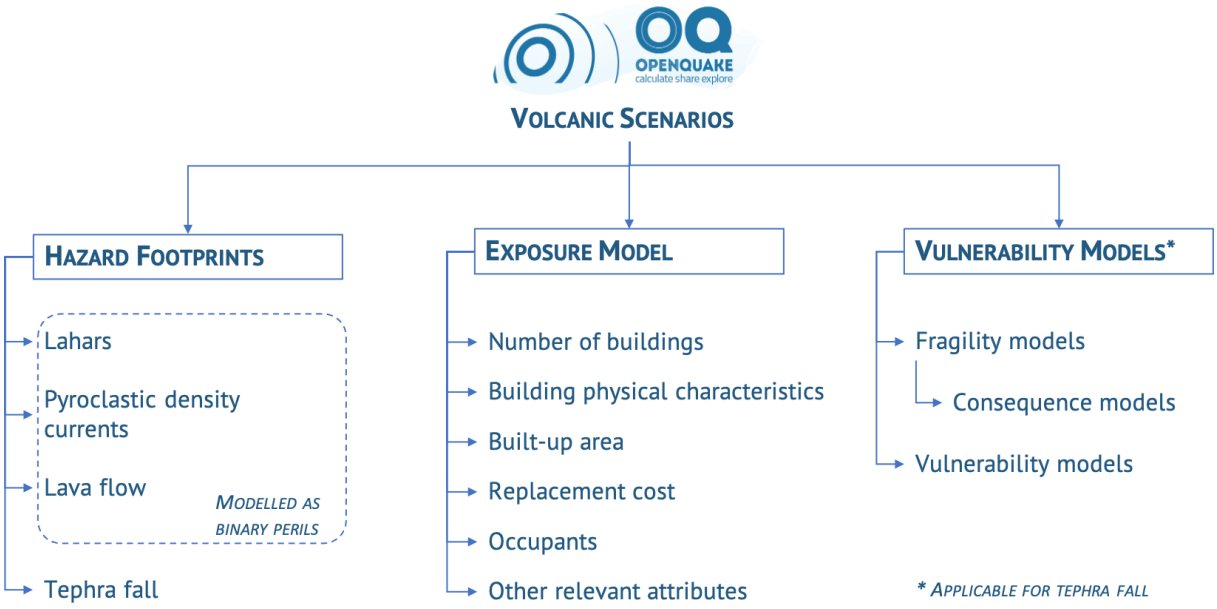


**Figure 1.** Input models for volcanic scenario calculations using the OpenQuake engine.

The current framework for earthquake and volcanic risk scenarios represents an initial effort to address both hazards. However, it does not account for the temporal duration of volcanic activity, which can severely impact agriculture, infrastructure, and community systems over extended periods – ranging from hours to years. Recent advancements in the OpenQuake engine now incorporate lifeline and connectivity risk assessments that could be applied to volcanic scenarios. Nevertheless, the case studies presented in this paper are limited to evaluating damage and economic losses to residential housing. Furthermore, the current implementation primarily addresses physical vulnerability, neglecting other critical dimensions of vulnerability in risk assessment, such as socio-economic and systemic vulnerabilities. Physical vulnerability remains the most extensively researched aspect of vulnerability in disaster risk reduction (Bonadonna et al., 2018, 2021; Deligne et al., 2022), and is a necessary precursor to evaluating broader impacts, including socio-economic and systemic dimensions (Bonadonna et al., 2018).

## 2.2 Volcanic hazard footprints

A hazard footprint refers to the spatial distribution, and sometimes intensity, of the volcanic hazard. Volcanic eruptions can involve multiple hazards, such as lava flows, lahars, gas emissions, tephra fall, and pyroclastic density currents. The hazard footprint delineates the geographic regions that are likely to experience the impacts of these hazards during a volcanic event as well as the intensity given the geographic location.

The implementation of the risk module of the OpenQuake engine is agnostic to the hazard under consideration, and therefore it can handle volcanic hazard footprints coming from any third-party tool. To facilitate the preparation of volcanic hazard footprints produced by third-party tools in the required OpenQuake format, the Input Preparation Toolkit (IPT) – *https://tools.openquake.org/ipt/*, originally developed to generate OpenQuake input files for earthquakes, has been extended to include a section for importing various types of volcanic hazard footprints. Figure 2 presents the IPT tab for "Volcano Scenarios".

The hazard footprint format in OpenQuake is typically a CSV file, where discrete points represent specific locations with their corresponding longitude, latitude, and hazard intensity values. When working with ShapeFiles in the IPT (Input Preparation Tool), a parameter called "discretisation distance" must be defined. This parameter controls the spacing between discrete points generated from the ShapeFile, ensuring that the layer is appropriately converted into the required CSV format for compatibility with OpenQuake.

To streamline the modelling process, the IPT was also extended to accept hazard footprints outputs for the most common modelling tools identified through a survey. This survey involved volcano modellers who detailed the types of analyses they perform, the volcanoes they consider, and the potential risk studies they conduct. In total, 13 scientists contributed to the survey, representing the SGC, PHIVOLCS, and the Rabaul Volcano Observatory (RVO) from Papua New Guinea. The summarized results are presented in Table 1.

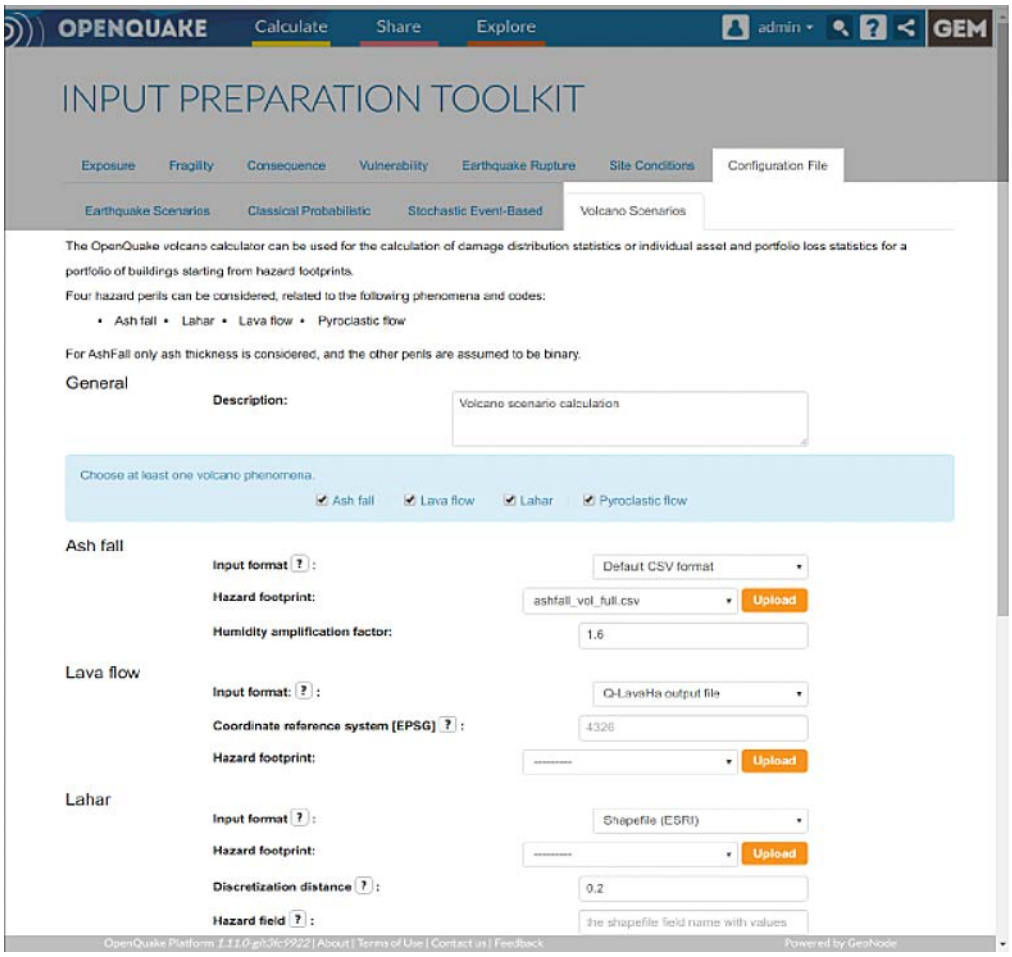


**Figure 2.** Volcanic scenarios tab in the Input Preparation Toolkit (IPT).

| Volcanic Hazard | Software | Organization Reference | Intensity (units) | Supported Outputs |
|---|---|---|---|---|
| Tephra fall | Ash3d | USGS (Mastin et al., 2013), (https://vsc-ash.wr.usgs.gov/ashgui/#/) | Tephra fall load (kPa) | ESRI Shapefile<br>ASCII<br>Raster |
| Lava Flow | Q-LavHa | Vrije Universiteit Brussel (Mossoux et al., 2016) (http://we.vub.ac.be/en/q-lavha) | Binary ("1"-affected, "0"-not affected) | ESRI Shapefile<br>ASCII<br>Raster |
| Pyroclastic Density Currents | Titan2D | Vhub and Buffalo University (Patra et al., 2005), (http://www.gmfg.buffalo.edu/) | Binary ("1"-affected, "0"-not affected) | ESRI Shapefile |
| Lahar | LaharZ | USGS, Schilling (1998), (https://pubs.er.usgs.gov/publication/ofr98638) | Binary ("1"-affected, "0"-not affected) | ESRI Shapefile |

**Table 1.** Volcanic hazards software outputs that can be directly used in the Input Preparation Toolkit (IPT).

The OpenQuake engine can accept volcanic hazard footprints generated by any external third-party tool. The software listed in Table 1 was selected to facilitate the direct use of its outputs when using the IPT. A brief overview of these compatible packages is provided below.

#### 2.2.1 Tephra fall

Ash3d (Mastin et al., 2013) is a three-dimensional modelling code. It is designed to simulate and forecast volcanic hazard of airborne tephra and tephra fall during volcanic eruptions. The simulation is done using a Eulerian model (Schwaiger et al., 2012), which sources wind observations from the Modern Numerical Weather Prediction (NWP) models to estimate tephra transport, dispersion and deposition. Ash3d provides a variety of specific outputs, depending on the modelling configuration (i.e. airborne or deposit). The output formats can be animations for Google EarthTM, GIS ESRI files or text files. Currently, the IPT supports the use of the ESRI ASCII (.asc) output file of the final tephra deposit thickness.

#### 2.2.2 Lava flow

Q-LavHA (Quantum-Lava Hazard Assessment) is a freeware multi-system QGIS plugin developed by Mossoux et al. (2016). This code simulates a lava flow inundation probability from one volcanic eruption on a Digital Elevation Model (DEM). The model can consider one or multiple, regularly spaced, eruptive vents, following the co-ordinates provided by the Smithsonian Institution Global Volcanism. Q-LavHA simulations produce as output a discrete representation of locations affected by the lava flow. The format of the output file follows the ESRI standards (georeferenced ASCII raster, .asc).

#### 2.2.3 Pyroclastic density currents

Titan2D is a modelling code developed by Patra et al. (2005). This program is designed to simulate volcanic flows (e.g. pyroclastic density currents, debris avalanches and landslides), combining numerical simulations of a mass flow with a detailed topographic representation through a Geographical Information System (GIS) interface. Titan2D employs a finite volume method for numerical integration, ensuring stable and accurate solutions over complex

terrain, while featuring a user-friendly graphical interface to set up simulations and visualize results. The outputs include maps and data of flow depth, velocity fields, runout distance, inundation area, dynamic pressure, and animated visualizations of pyroclastic density currents.

#### 2.2.4 Lahar

LaharZ is a GIS plugin (ArcMAP toolbox for ArcGIS v.9 or later) created by Schilling (2014). It is designed to estimate distal inundation zones over a three-dimensional detailed topography (DEM). The distal zones are an interpretation of potential lahar inundation areas (volumes) over one or more stream drainages. The LaharZ output format is a 2D georeferenced surface following ESRI shapefile standards.

## 2.3 Exposure model

In the OpenQuake engine, an exposure model represents the built environment and its occupants, incorporating details such as geographic location, quantity, and physical characteristics of assets. While the OpenQuake engine can handle exposure models for buildings, infrastructure, and lifelines in earthquake analysis, its current implementation for volcanoes has been only tested on buildings. Therefore, for volcanic scenarios, the exposure model may include information such as the number of buildings, construction materials, roof types, average built-up area, and average replacement cost. Additionally, exposure models can account for population occupancy patterns (e.g. the number of occupants during the day, at night, and in transit). In certain cases, socio-economic variables and demographic information may also be incorporated to assess physical and social risks to buildings and their occupants. Expanding OpenQuake's capabilities to incorporate other exposed elements, such as infrastructure and lifelines, would significantly broaden the scope of volcanic risk assessments.

The OpenQuake engine uses a unified format for exposure models across both earthquake and volcanic hazards, and across the different calculators, ensuring compatibility. The exposure model consists of CSV files listing asset-specific information, complemented by an XML file containing metadata that provides general details about the exposure. The asset data is represented as discrete points with longitude and latitude coordinates assigned to each asset. Each asset is described by key attributes such as the number of buildings, a taxonomy class (which relates to the building's vulnerability to the specific hazard), area, cost, and the number of occupants. The exposure model is highly flexible, allowing users to expand or tailor the asset data to meet the specific requirements of the analysis being conducted.

For earthquakes exposure models, a relatively coarse spatial resolution (e.g. at the district or neighbourhood level) is often sufficient when the ground shaking and soil characteristics are relatively uniform within the resolution considered, and the event affects large regions extending hundreds of kilometers from the rupture. On the other hand, exposure models for volcanic risk assessment typically require higher spatial resolutions due to the complex and multi-hazard nature of volcanic eruptions, which can affect population and infrastructure at varying geographical scales. For example, lahars follow the topographic slopes and tend to concentrate around rivers and streams, while lava flows typically impact areas within a limited distance from the crater (usually less than 100 km). Tephra fall, like earthquakes, can affect sites hundreds of kilometres away from the volcano. Moreover, for reliable risk estimation, the building characteristics in the exposure model must align with the specific hazard under consideration. For example, when considering tephra fall, it is crucial to include detailed information about the roof material and type (e.g. roof pitch, structural supports and roof conditions), as the vulnerability of buildings to tephra fall depends directly on these attributes.

## 2.4 Fragility model

Fragility models are required for assessing building damage impact for calculations that include non-binary perils, i.e., tephra fall. A fragility model defines a set of fragility functions for different building classes, with each function describing the probability of exceeding a set of damage states given the intensity of the hazard under consideration, e.g. tephra fall load in kPa. It is necessary to provide a fragility function for each building typology

present in the exposure model. The fragility functions can be defined using either a discrete or a continuous format, and the fragility model file can include a mix of both types of fragility functions.

Although tephra fall is one of the most extensively studied volcanic hazards due to its widespread occurrence and significant impact on large areas (Blong et al., 2017), there are surprisingly few quantitative fragility models available for this hazard (see the mini-review by Hayes et al., 2024). Table 2 summarizes the fragility models considered for the selection of the specific model in each case study. This scarcity of fragility models for volcanic risk assessment stands in stark contrast to earthquake risk, where hundreds of models are available at local, national, and regional scales (Yepes-Estrada et al., 2016).

| Authors | Study | Roof/Building class | Description |
|---|---|---|---|
| Blong et al., 2017 | Existing vulnerability functions developed for volcanic tephra fall impact on buildings and apply them to a hypothetical building portfolio impacted by a modern-day Tambora 1815 eruption scenario. The study includes results from different experts. Tephra density is assumed to be 1,620 kg/m$^3$. | W1-NonEng-H | Light frame wood, non-engineered, roof pitch ≥ 35° |
| | | W2/S3-NonEng-M | Commercial and industrial, non-engineered, roof pitch = 6-35° |
| | | C3M/RMM-Eng-M | Concrete fame/reinforced masonry, engineered, roof pitch < 6° |
| | | URML-M | Unreinforced masonry, roof pitch = 6-35° |
| | | PBC-L | Post and beam construction, roof pitch < 6° |
| Jenkins et al., 2014 | Exposure and vulnerability assessment for two case study areas: Kanlaon volcano in the Philippines, and Fogo volcano in Cape Verde. Fragility curves were developed for broad building typologies, applicable globally. | A_af | Weak timber boards on timber rafters/trusses, metal sheet roofs on timber rafters/trusses in poor condition |
| | | B_af | Long-span roofs with metal sheets or fiber-reinforced concrete sheets |
| | | C_af | Metal sheet roofs on timber rafters/trusses in average condition, tiles on timber rafters/trusses in average condition |
| | | D_af | Metal sheet roofs on timber rafters/trusses in good condition, strong timber on timber rafters/trusses in average or good condition |
| | | E_af | Flat RC roof designed for access and in general good condition |
| | | Type A | Roofs with rafters of 50 mm × 75 mm spaced at 200 mm and spanning 2 m between purlins of 100 mm × 150 mm covered with boarding old or new tiles that were visibly in good condition |

| Authors | Study | Roof/Building class | Description |
|---|---|---|---|
| Pomonis et al., 1999 | Study the risks to human settlements of a future eruption of the Furnas Volcano in Azores (Portugal). The average compacted wet tephra density assumed was 1,200 kg/m$^3$. | Type B | Roofs with rafters of 35 mm × 55 mm spaced at 250 mm and spanning 1.35 m between purlins of 75 mm × 125 mm. Covered with boarding new tiles or asbestos sheets that were visibly in good condition |
| | | Type C | Roofs with rafters of 50 mm × 75 mm spaced at 200 mm and spanning 2 m between purlins covered with boarding old tiles that were as type A but visibly in poor condition |
| | | Type D | Roofs with rafters of 35 mm × 55 mm spaced at 250 mm and spanning 1.35 m between purlins covered with boarding new tiles or asbestos sheets that were as type B but visibly in poor condition |
| Spence et al., 2005 | Fragility curves are presented for roofs in Europe, and applied to the area around Mt. Vesuvius in southern Italy. | Weak roof [WE] | Sheet roofs, old or in poor condition tiled roof |
| | | Medium weak roof [MW] | Sheet roof on timber, average or good quality tiled roof on timber rafters or trusses |
| | | Medium strong roof [MS] | Flat RC roof, sloping RC roof |
| | | Strong roof [ST] | Flat RC roof designed for access, good quality construction younger than 20 years |
| Torres-Corredor et al., 2017 | Fragility functions for the Galeras volcano in Colombia assuming different roof configurations and characteristics. The tephra density was assumed to be 1,250 kg/m$^3$. | Weak roof | |
| | | Moderate roof | |
| | | Heavy roof | |
| | | Slab roof | |
| Zuccaro et al., 2008 | Risk assessment for a Plinian I eruptive scenario of the Mt. Vesuvius in Italy. The tephra density was assumed to be 1,000 kg/m$^3$. | Ar | Weak-pitched wooden roof |
| | | Br | Flat standard wooden roof, Reinforced concrete flat roof, |
| | | C1r | Flat RC roof older than 20 years |
| | | C2r | Flat RC roof younger than 20 years |
| | | Dr | Recent flat RC roof, recent pitched RC roof, recent steel pitched roof |

**Table 2.** Fragility models for roof damage due to tephra fall considered in this study.

# 3. Case study 1: VEI 3-4 scenario for Nevado del Ruiz volcano, Colombia

In collaboration with the SGC, we tested the proposed methodology for a deterministic scenario risk assessment for the "Nevado del Ruiz" volcano in central Colombia.

## 3.1 Volcanic hazard footprints

The SGC developed national hazard maps for this volcano (SGC, 2015; Ceballos et al., 2016) where hazard footprints are available for tephra fall (thickness and load), lahars, lava flows, and pyroclastic density currents. These footprints are shown in Fig. 3, which represents a scenario with characteristics similar to a VEI 3-4.

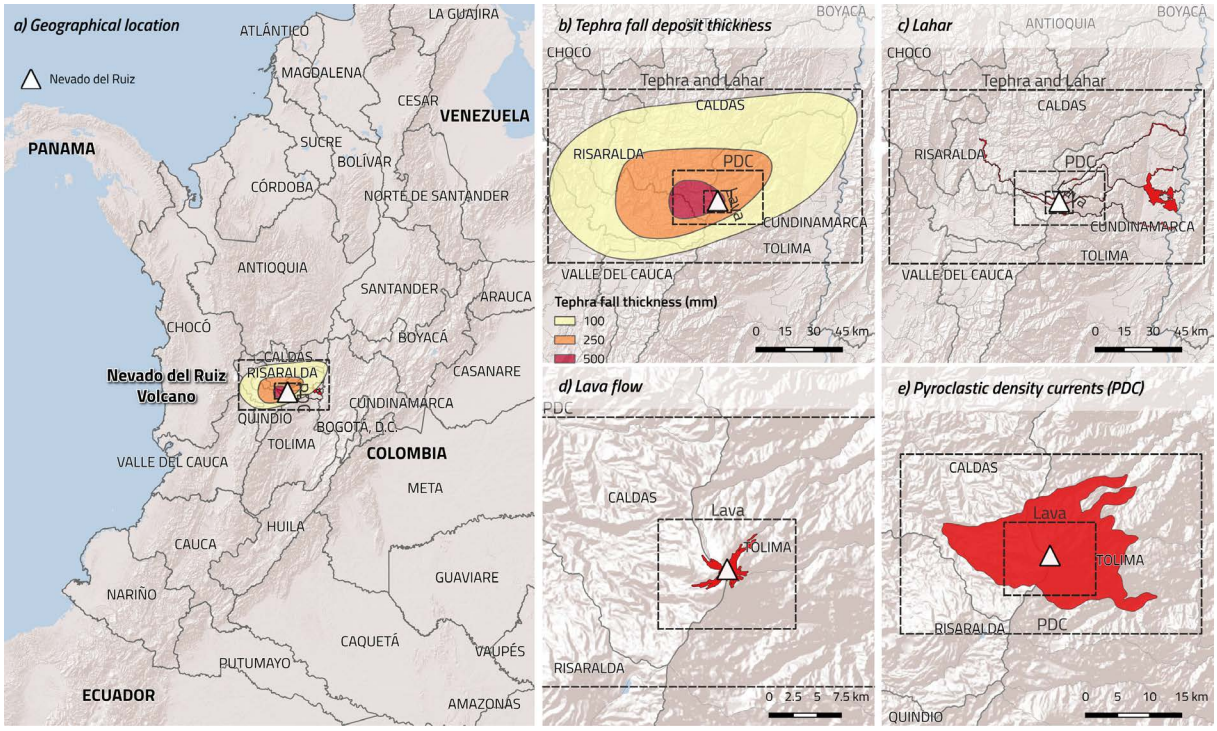


**Figure 3.** Hazard footprint for Nevado del Ruiz volcano deterministic case study: (a) geographical location, from (b) to (e) hazard footprints for (b) tephra fall deposit thickness, (c) lahar, (d) lava flow and (e) pyroclastic density currents. Red footprints for lahar, lava flow and pyroclastic density currents represent inundation.

## 3.2 Exposure and fragility models

An updated and improved exposure model for the residential buildings of Colombia was developed in collaboration with the SGC. The model was based on the GEM Global Seismic Risk Model (Silva et al., 2020). Information regarding the roof type (weak roof, slab roof, moderate and heavy roof) was incorporated, as well as information from the national census survey (DANE, 2005) at the block level and taking into account national results from previous census surveys (from 1993).

In this context, since the spatial resolution of the exposure model (block level) in the urban areas was suitable for volcanic risk assessment, only the spatial resolution for the rural buildings was improved using satellite imagery with rivers, lakes, roads, night-time lights and population density, as well as crowd-sourced datasets (e.g. OpenStreetMap data) to disaggregate to a finer resolution of 250 m. This procedure can be applied to any country in the world (Yepes-Estrada et al., 2023), which facilitates the extension of the current methodology to other regions.

In addition, the SGC collected detailed information from the geographic information database of Colombia, available through the IGAC (Instituto Geográfico Agustin Codazzi, https://igac.gov.co/) at a scale 1:25000, with the exact location of the residential buildings in the surroundings of the volcano, covering around 36,000 housing units, all of which were located in rural areas. This information was incorporated into the residential exposure model. Figure 4 presents the location and number of the dwellings in the volcano's surroundings. The resulting exposure model indicates that more than 170 municipalities in the country are located within a 100 km radius of the volcano's crater, representing more than 3.5 million residents in over 1.35 million residential dwellings, with an estimated replacement value of 90 USD billion. The orange and red colours on the map highlight the location of the urban centres close to the volcano.

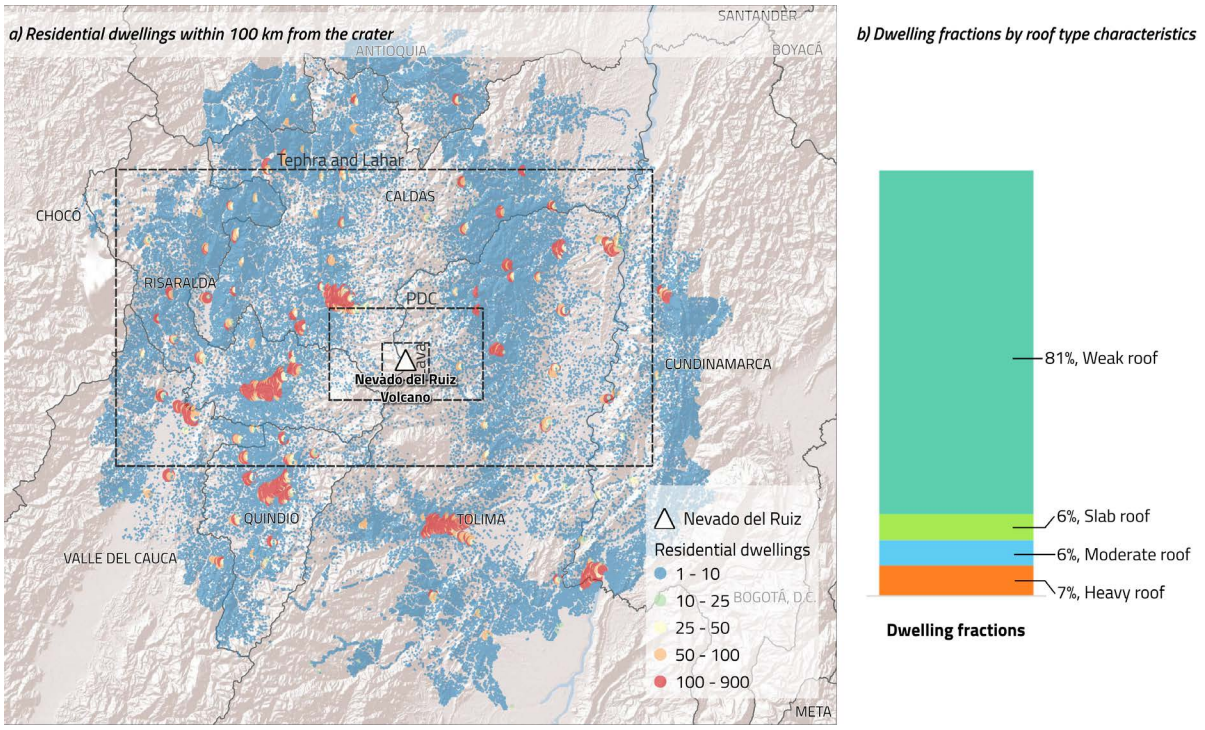


**Figure 4.** Nevado del Ruiz volcano (a) distribution of residential dwellings within 100 km by number of units; (b) Dwelling fractions by roof type characteristics.

For the estimation of the tephra fall load impact, the most applicable function for this case study was chosen from the tephra fall fragility functions of Table 2, with the functions developed by Torres-Corredor et al. (2017), for the Galeras volcano in Colombia, selected as they were developed for comparable Colombian building typologies. The set of fragility functions accounts for roof collapse probability conditioned on tephra fall load for four roof types: light roofs, moderate roofs, heavy roofs, and reinforced concrete slab roofs.

## 3.3 Volcanic scenario risk assessment results

Considering a deterministic VEI 3-4 scenario for Nevado del Ruiz volcanic hazard footprints, the volcano risk calculator of the OpenQuake engine was used to quantify the potential impact on residential buildings in Colombia. The information presented below used the exposure model indicated in the previous section, which will require updating for future risk studies. Table 3 presents the summary of the affected dwellings, affected occupants and economic losses. For the analysis, it was assumed a "humidity amplification factor" of 2 for tephra load in wet conditions.

Figure 5 presents examples of the maps and risk metrics generated for pyroclastic density currents, lahar and tephra fall in dry and wet conditions aggregated at the municipal level.

| Volcanic hazard | Affected dwellings (Thousands) | Affected occupants (Thousands) | Economic losses (Million COP) |
|---|---|---|---|
| Tephra fall (dry) | 66,847 | – | 325,443 |
| Tephra fall (wet) | 171,908 | – | 896,147 |
| Lahar | 7,977 | 16,047 | 475,630 |
| Lava flow | 1 | 4 | 42 |
| PDC | 218 | 1,110 | 14,236 |

**Table 3.** Summary of affected dwellings, occupants and economic losses for Nevado del Ruiz volcano.

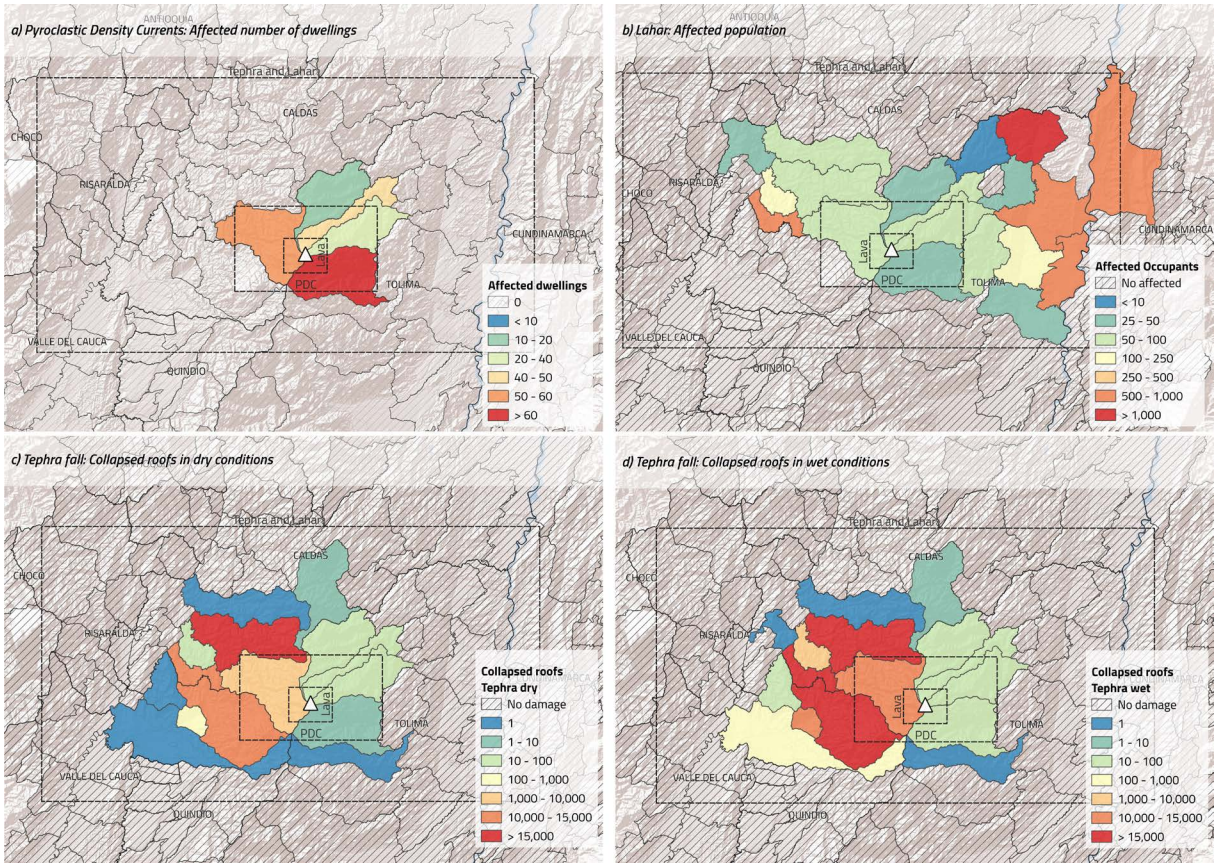


**Figure 5.** Risk maps using OpenQuake for the El Ruiz volcano in Colombia (a) dwellings affected by pyroclastic density currents, (b) occupants affected by lahar, (c) collapsed roofs by tephra fall in dry conditions, and (d) collapsed roofs by tephra fall in wet conditions.

## 4. Case study 2: Probabilistic tephra dispersal modelling for the Pinatubo volcano, Philippines

In collaboration with the EOS and PHIVOLCS, a VEI 6 scenario risk assessment using probabilistic tephra fall hazard simulations was carried out for Pinatubo volcano in northern Luzon, Philippines.

## 4.1 Volcanic hazard footprints

Jenkins et al. (2019) simulated the Pinatubo eruption of 1991 as a probabilistic scenario using the freely available and well-established Tephra2 model (Connor et al., 2006). Tephra2 was run through the open-source probabilistic wrapper TephraProb (Biass et al., 2016) to provide an easy-to-use approach for simulating, processing and visualizing large numbers of potential eruption outcomes. Credible ranges for a Volcanic Explosivity Index (VEI) 6 eruption were established from a range of sources, with bounds provided by the VEI classification, the Pinatubo 1991 eruption, and the literature. 15,000 simulations were run for the scenario, accounting for seasonal effects and variation in source parameters, e.g. plume height, erupted mass, and grain size distributions. Analysing the results of the individual footprints shows that tephra is typically dispersed towards the west, but that the area affected is dependent upon the sampled source parameters and meteorological conditions. Three main outputs were produced: 1) Probability maps: the probability of exceeding a certain load threshold for each grid cell; 2) Isomass maps: the tephra load associated with certain probability percentiles for each grid cell; and 3) Hazard curves: that describe the probability of exceeding the range of tephra fall loads at individual locations.

Figure 6 presents examples of the generated results. The top-left map indicates the probability of exceeding ground tephra accumulations of 10 kg/m$^2$, with contours showing the probability of exceeding the loading threshold,

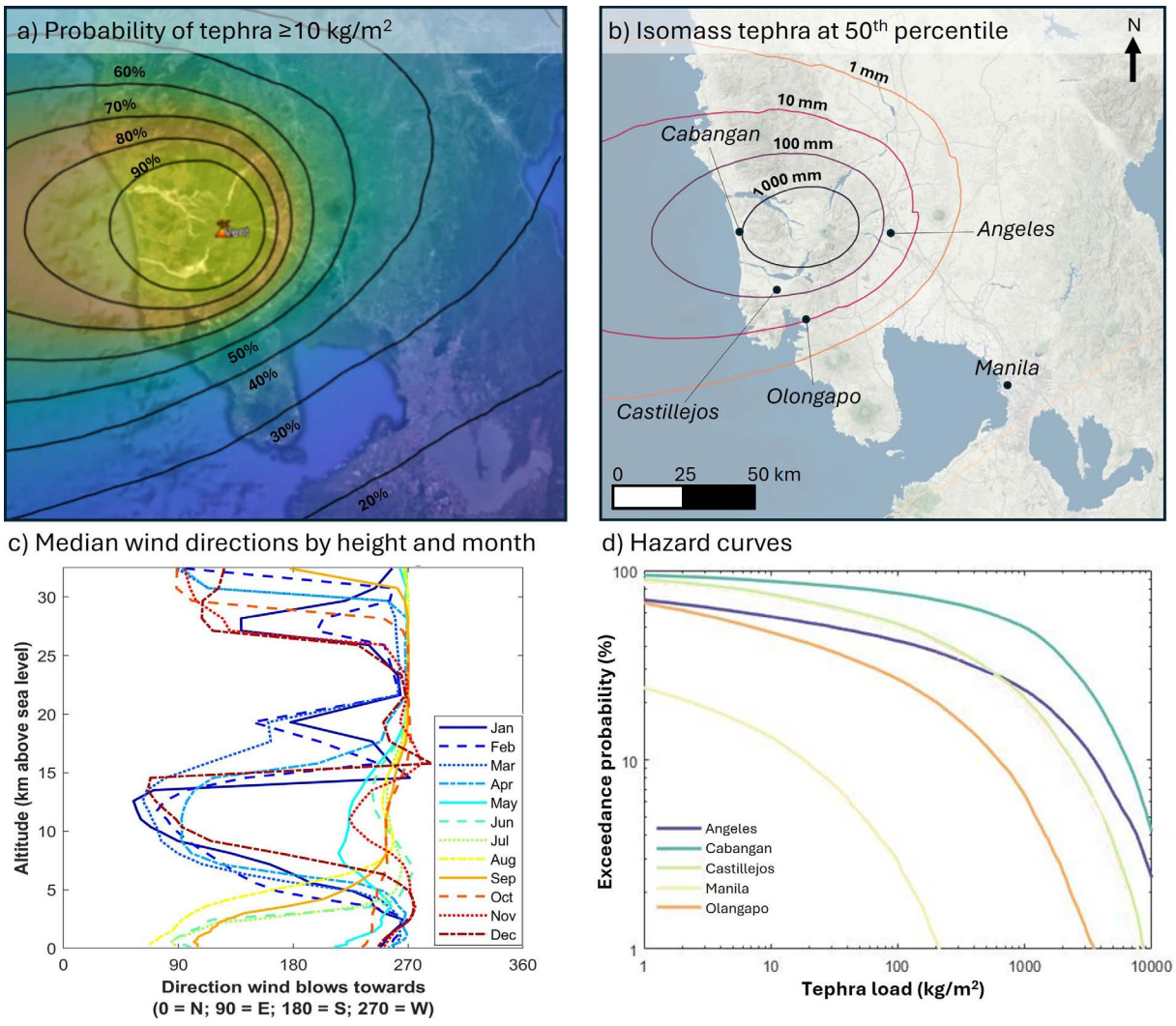


**Figure 6.** Given a VEI 6 style eruption from Pinatubo. (a) contour probability map (20% through 90%) for exceeding 10 kg/m$^2$ tephra accumulation; (b) isomass map for the 50% probability exceedance; (c) median wind directions per height and month; (d) hazard curves. Seasonality is not shown in these plots, with whole year wind conditions considered. Source Jenkins et al. (2019).

with the closest contour to the vent ⩾ 90% and each contour then at 10% intervals. The top-right map shows the isomass (tephra load associated with a given percentile) using fixed exceedance probabilities of 50%, where contours closest to the vent refer to the 1000 kg/m$^2$ loading, followed by the 100, 10, and 1 kg/m$^2$ loading thresholds, and the minimum tephra fall load shown is 0.1 kg/m$^3$. The bottom-left figure shows the median wind speed directions blowing towards Pinatubo with height above sea level for each month. Finally, the bottom-right figure shows the hazard curves computed for a small number of selected cities, with no seasonality shown.

The current implementation of the OpenQuake engine for volcanic risk scenarios does not natively support probabilistic outputs, such as hazard curves at specific locations or hazard maps for a given probability of exceedance. Instead, the software can process hazard footprints generated by external tools (e.g. Tephra2), provided the data are in the required format. Using this approach, 15,000 simulations accounting for seasonality and variability in source parameters were conducted to assess tephra fall risk for the Pinatubo eruption. From these simulations, mean risk results were then derived.

## 4.2 Exposure and vulnerability models

The exposure model for the Philippines was also improved using a similar approach as the one described for Colombia in the preceding case study. Information from the 2010 Population and Housing Census, Philippine Statistic Authority (https://psa.gov.ph/), at the municipal level was retrieved for residential buildings, which reported the number of dwellings by material of the walls and material of the roof at the municipality level. The available census data comprised information about the material of the roof classified into eight categories. By combining the building classification for earthquake hazard with the material of the roof, the most likely roof class was assigned based on expert judgment. The categories to classify the roof performance are closely related to the roof fragility models

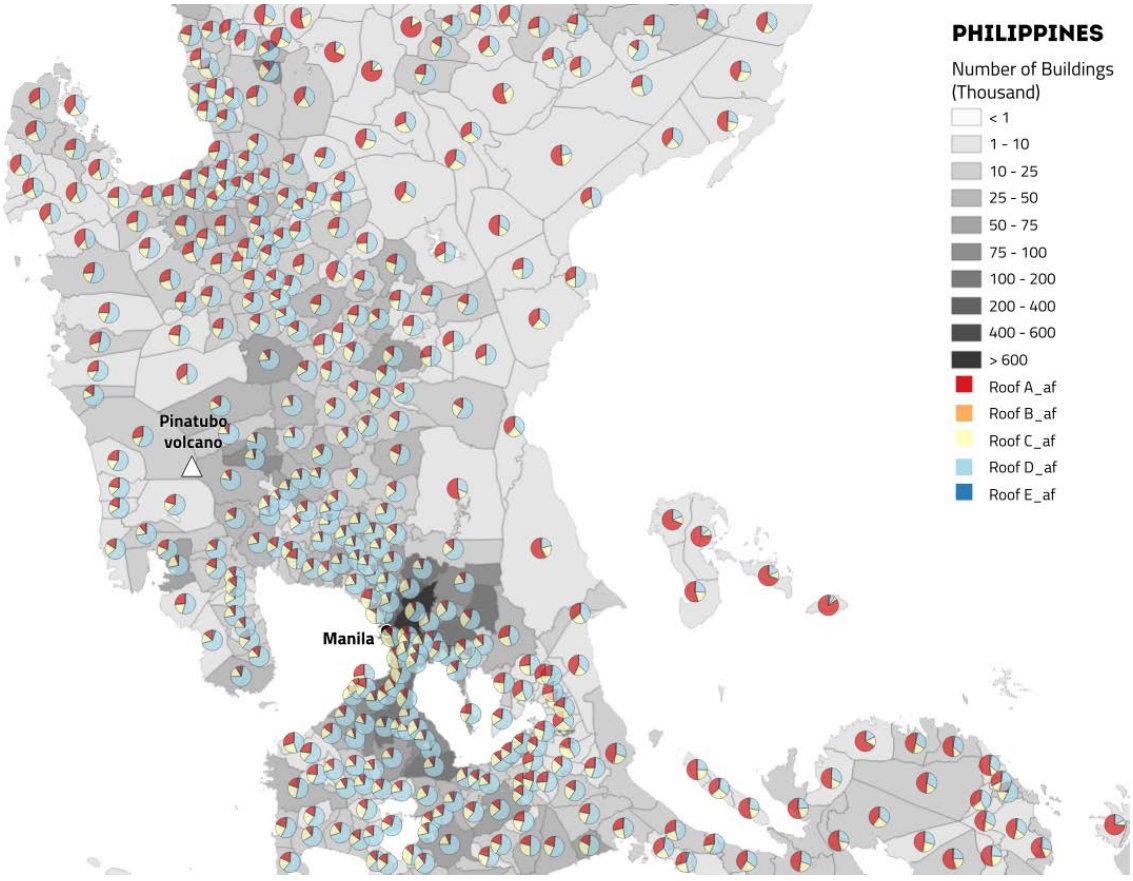


**Figure 7.** Number of residential buildings and distribution of roof classes (pie charts) in the surrounding area of the Pinatubo volcano. See Jenkins et al., 2014 row in Table 2 for descriptions.

available, see Table 2. In the case of the Philippines, the fragility model proposed by Jenkins et al. (2014) was used as it had been refined to Filipino building typologies. This study provides information regarding the collapse roof probability of exceedance due to tephra load for five categories of roof, from A to E, with A being the most fragile roof type under tephra fall load and E being the least fragile (see Table 2).

At the national level, it was found that the predominant roof classes are types D, A, and C representing 42%, 33%, and 22% of the buildings respectively. Categories B and E are not common, each one representing 1% of the total buildings. In contrast, if the fraction of roof classes is estimated based on the building replacement cost instead of the number of buildings, the fractions are 59%, 21%, and 15% for types D, A, and C respectively; while type E moves up to 5% and type B stays at 1%. Figure 7 shows the distribution of roof type across the affected area, where it can be observed that closer to the highly urbanized areas, like Manila, the roofing class D is predominant (good condition metal sheet; colour green in the pie charts), while toward the North and East, the predominant roof types are of class A (weak timber or poor condition metal sheet; colour red in the pie charts).

## 4.3 Volcanic scenario risk assessment results

This section presents the results of volcanic scenario risk assessment considering uncertainty through simulations based on a probabilistic model for a VEI 6 eruption scenario of the Pinatubo tephra fall volcano. Three potential weather conditions were contemplated: i) eruption during the dry season (5,000 simulations); ii) eruption during the rainy season (5,000 simulations); and iii) eruption for the whole year (5,000 simulations).

Using the OpenQuake engine, each of the 15,000 tephra fall load simulations were combined with exposure and fragility models, accounting for specific building and roof types, to assess the probability of roof damage and estimate potential economic losses. Table 4 presents the summary of the mean number of collapsed roofs and economic losses for the three considered weather conditions.

| Season | Mean collapsed roofs (Thousands) | Mean economic losses (Million USD) |
|---|---|---|
| Dry | 242 | 1,149 |
| Rainy | 384 | 1,812 |
| All year | 324 | 1,529 |

**Table 4.** Summary of mean number of collapsed roofs and economic losses for the Pinatubo simulations.

The distribution of the number of collapsed roofs and the corresponding collapse ratios are presented in Fig. 8 for the three considered weather conditions, and for economic losses, similar figures are presented in Fig. 9. As expected, larger collapse ratios are encountered closer to the volcano crater, given that the roof classes were generally similar across the affected area.

When comparing roof collapses and economic losses across various building classes throughout the year, buildings with predominant material of reinforced and confined masonry were the most impacted. This is primarily due to their prevalence as the dominant construction practice in the country, accounting for 56% of the affected roofs and 71% of the direct economic losses. The mean ratio of collapsed roofs to total buildings and of economic loss to total value exposed within each province/municipality shows that the larger number of buildings and economic losses are concentrated near cities in larger municipalities While the greatest proportion of impacts, on average, was concentrated close to the volcano.

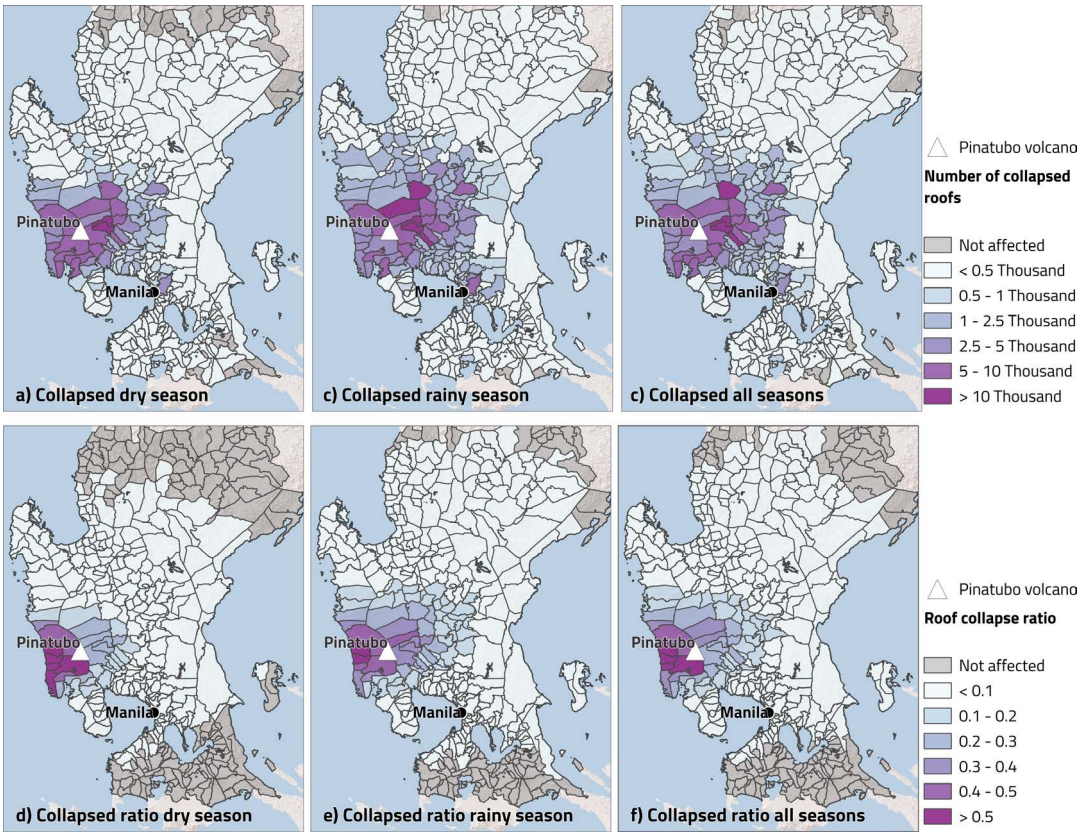


**Figure 8.** Distribution of mean number of collapsed roofs (a to c), and mean roof collapse ratio (d to f). Roof collapse ratio is the mean total number of collapsed roofs in each municipality divided by the total number of buildings.

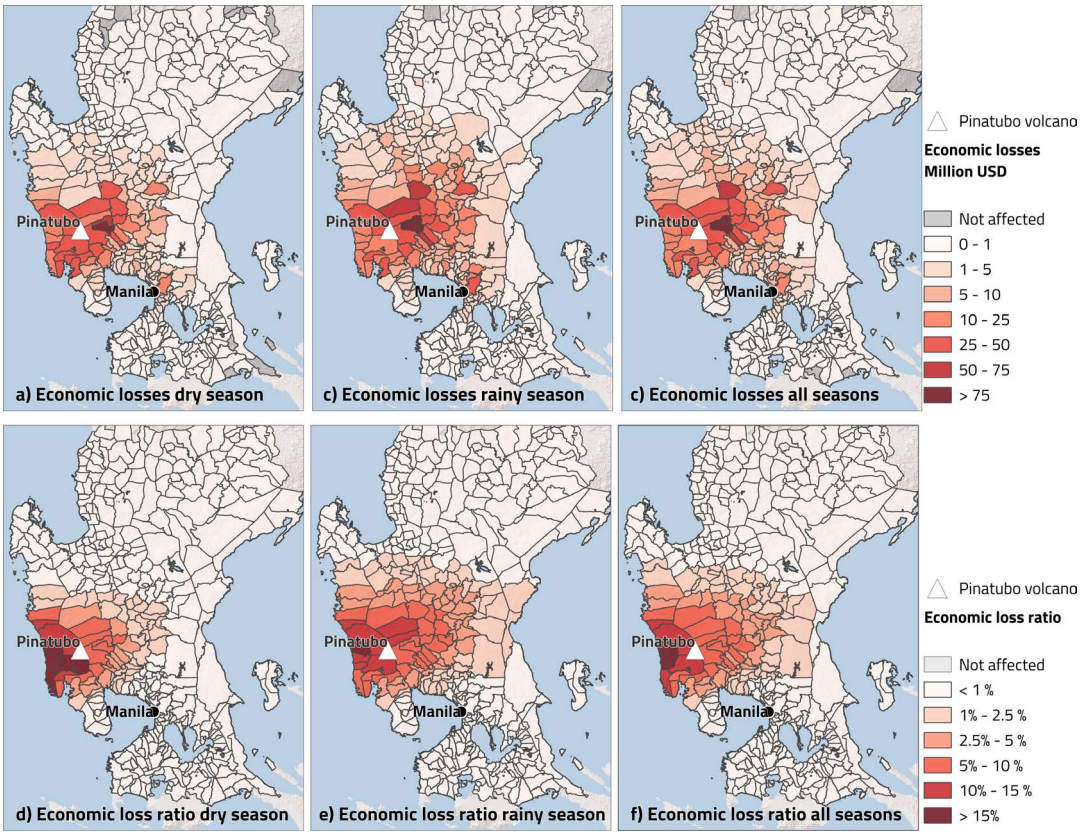


**Figure 9.** Distribution of the mean economic loss (a to c), and mean loss ratio (d to f) due to roof collapse in buildings.

## 5. Conclusions

This study integrates volcanic risk scenario assessment within the OpenQuake engine, extending its established capabilities for earthquake risk assessment to encompass deterministic and probabilistic scenario risk computations for volcanic hazards. By developing a common framework for assessing the impact of earthquakes and volcanoes on the built environment (buildings), we provide a versatile and robust tool for disaster risk management. However, fully capturing the complexity of volcanic risk assessment remains challenging, particularly due to the dynamic variations in hazard, exposure, and vulnerability, as well as their interconnected and compounding effects over time and space.

The application of this framework to the Nevado del Ruiz, Colombia and Pinatubo, Philippines volcanoes demonstrates its effectiveness in handling multiple hazard scenarios and delivering valuable insights for risk mitigation, preparedness, and response. However, it is essential to collaborate with local scientists to better characterize not only the hazard but also the exposure and vulnerability. These examples illustrate how local knowledge can significantly enhance the spatial resolution and detail of the exposure model. By incorporating key elements such as roof materials, structural types (pitch, openings, spans, supports), and conditions, the quality and reliability of the analysis can be improved.

This work represents an advancement in combining state-of-the-art earthquake and volcano risk modelling and assessment within a single tool, opening up the capability of using compatible exposure models to assess the risks from the different hazards.

**Data availability statement.** Data can be downloaded at https://www.globalquakemodel.org/proj/crave for Nevado del Ruiz case study, and at https://doi.org/10.21979/N9/7NTU8M for Pinatubo case study.

**Acknowledgements.** The work presented in the current manuscript was supported by the United States Agency for International Development (USAID) through the Collaborative Risk Assessment for Volcanoes and Earthquakes (CRAVE) project. We extend our gratitude to the numerous scientists who contributed their expertise and insights. Special thanks to Julio Antonio García Peláez formerly at the GEM Foundation, to the Colombian Geological Survey (SGC), the Rabaul Volcano Observatory (RVO) in Papua New Guinea, the Philippine Institute of Volcanology and Seismology (PHIVOLCS), the British Geological Survey (BGS), the Earth Observatory of Singapore (EOS), University of Edinburgh, Volcano Disaster Assistance Program (VDAP), and other collaborating institutions for their invaluable support and participation. Their dedication and collaboration were instrumental in the success of this project.

## References

Alberico, I., P. Petrosino and L. Lirer (2011). Volcanic hazard and risk assessment in a multi-source volcanic area: the example of Napoli city (Southern Italy), Nat. Hazards Earth Syst. Sci., 11, 4, 1057-1070, doi:10.5194/nhess-11-1057-2011.

Allen, T. I., J. D. Griffin, M. Leonard, D. J. Clark et al. (2020). The 2018 national seismic hazard assessment of Australia: Quantifying hazard changes and model uncertainties, Earthq. Spectra, 36, 1 suppl., 5-43, doi:10.1177/8755293019900777.

Arcila, M., J. García, J. Montejo, J. Eraso et al. (2020). Modelo nacional de amenaza sísmica para Colombia, Bogotá: Servicio Geológico Colombiano y Fundación Global Earthquake Model, doi:10.32685/9789585279469.

Baxter, P. J., R. Boyle, P. Cole, A. Neri et al. (2005). The impacts of pyroclastic surges on buildings at the eruption of the Soufrière Hills volcano, Montserrat, Bull. Volcanol., 67, 292-313, doi:10.1007/s00445-004-0365-7.

Beauval, C., J. Marinière, H. Yepes, L. Audin et al. (2018). A New Seismic Hazard Model for Ecuador, Bull. Seismol. Soc. Am., 108, 3A, 1443-1464, doi:10.1785/0120170259.

Biass, S., C. Bonadonna, L. Connor and C. Connor (2016). TephraProb: a Matlab package for probabilistic hazard assessments of tephra fallout, J. Appl. Volcanol., 5, 1, 10, doi:10.1186/s13617-016-0050-5.

Blong, R. J., P. Grasso, S. F. Jenkins, C. R. Magill et al. (2017). Estimating building vulnerability to volcanic ash fall for insurance and other purposes, J. Appl. Volcanol., 6, doi:10.1186/s13617-017-0054-9.

Bonadonna, C., S. Biass, E. S. Calder, C. Frischknecht et al. (2018). 1st IAVCEI/GVM Workshop: From Volcanic Hazard to Risk Assessment, Geneva, 27-29 June 2018, https://theghub.org/resources/4498.

Bonadonna, C., C. Frischknecht, S. Menoni, F. Romerio et al. (2021). Integrating hazard, exposure, vulnerability and resilience for risk and emergency management in a volcanic context: the ADVISE model, J. Appl. Volcanol., 10, 7, doi:10.1186/s13617-021-00108-5.

Brown, S. K., S. F. Jenkins, R. S. J. Sparks, H. Odbert et al. (2017). Volcanic fatalities database: analysis of volcanic threat with distance and victim classification, J. Appl. Volcanol., 6, 1-20, doi:10.1186/s13617-017-0067-4.

Calderon, A., C. Yepes-Estrada, C. Celi, J. Marrero et al. (2022). Evaluación de Riesgo Sísmico para el Distrito Metropolitano de Quito, GEM-TREQ Reporte Técnico D2.6.1, doi:10.13140/RG.2.2.16762.16322.

Ceballos, J. A., L. M. Martínez and I. Zuluaga (2016). Evaluación de la amenaza de la tercera versión del mapa de amenaza del Volcán Nevado del Ruiz (2015), Servicio Geológico Colombiano, 221, Manizales, Colombia, https://recordcenter.sgc.gov.co/B23/696_2020TercVersionMAVNR/Documentos/Pdf/EvalAmenVNR.pdf.

Chan, C. H., K. F. Ma, J. B. H. Shyu, Y. T. Lee et al. (2020). Probabilistic seismic hazard assessment for Taiwan: TEM PSHA2020, Earthq. Spectra, 36, 1 suppl., 137-159, doi:10.1177/8755293020951587.

Connor, L. J. and C. B. Connor (2006). Inversion is the key to dispersion: understanding eruption dynamics by inverting tephra fallout, in Statistics in Volcanology H. M. Mader, S. G. Coles, C. B. Connor and L. J. Connor (Eds.), Geol. Soc. Spec. Publ., 231, doi:10.1144/IAVCEI001.18.

DANE (2005). Censo General 2005, Departamento Administrativo Nacional de Estadística, Colombia, https://www.dane.gov.co/.

Deligne, N. I., S. F. Jenkins, E. S. Meredith, G. S. Leonard et al. (2022). From anecdotes to quantification: advances in characterizing volcanic eruption impacts on the built environment, Bull. Volcanol., 84, 7, doi:10.1007/s00445-021-01506-8.

EM-DAT CRED UCLouvain (2024). Number of deaths from disasters, Data includes disasters recorded up to April 2024, Our World in Data based on EM-DAT, CRED, UCLouvain, D. Guha-Sapir, Brussels, Belgium, www.emdat.be.

GAR Global Assessment Report (2015). Global Assessment Report on Disaster Risk Reduction 2015, Making Development Sustainable: The Future of Disaster Risk Management, Geneva, United Nations International Strategy for Disaster Reduction (UNISDR), www.preventionweb.net/english/hyogo/gar/2015.

Gerstenberger, M. C., S. Bora, B. A. Bradley., C. Di Caprio et al. (2022). The 2022 Aotearoa New Zealand National Seismic Hazard Model: Process, Overview and Results, Bull. Seismol. Soc. Am., 114, 1, 7-36, doi:10.1785/0120230182.

Hayes, J. L., R. H. Fitzgerald, T. M. Wilson, A. Weir et al. (2024). Linking hazard intensity to impact severity: mini-review of vulnerability models for volcanic impact and risk assessment, Front. Earth Sci., 11, 1-8, doi:10.3389/feart.2023.1278283.

Hobbs, T. E., J. M. Journeay, A. Rao, M. Kolaj et al. (2023). A national seismic risk model for Canada: methodology and scientific basis, Earthq. Spectra, 39, 3, 1410-1434, doi:10.1177/87552930231173446.

Irsyam, M., P. R. Cummins, M. Asrurifak, L. Faizal et al. (2020). Development of the 2017 national seismic hazard maps of Indonesia, Earthq. Spectra, 36, 1 suppl., 112-136, doi:10.1177/8755293020951206.

Jenkins, S. F., R. Spence, J. Fonseca, R. Solidum et al. (2014). Volcanic risk assessment: Quantifying physical vulnerability in the built environment, J. Volcanol. Geotherm. Res., 276, 105-120, doi:10.1016/j.jvolgeores.2014.03.002.

Jenkins, S. F., T. M. Wilson, C. Magill, V. Miller et al. (2015). Volcanic ash fall hazard and risk, in Global volcanic hazards and risk, Cambridge University Press, 173-222, doi:10.1017/CBO9781316276273.005.

Jenkins, S. F., J. C. Phillips, R. Price, K. Feloy et al. (2015b). Developing building-damage scales for lahars: application to Merapi volcano, Indonesia, Bull. Volcanol., 77, 1-17, doi:10.1007/s00445-015-0961-8.

Jenkins, S. F., D. Biass and C. J. Rui (2019). Report to accompany tephra fall footprints, for use in the CRAVE project, GEM Foundation.

Kolaj, M., S. Halchuk and J. Adams (2023). Sixth generation seismic hazard model of Canada: Final input files used to generate the 2020 National Building Code of Canada seismic hazard values, Geol. Surv. Canada Open File, 8924, ed. Version 1.0, 14, doi:10.4095/331387.

Loughlin, S. C., R. S. J. Sparks, S. K. Brown, S. F. Jenkins et al. (2015). Global volcanic hazards and risk, Cambridge University Press, 93, doi:10.1017/CBO9781316276273.

López, A., L. Mixco, M. López, S. Flores et al. (2024). Assessing seismic risk for effective disaster management at the department level in El Salvador, Proceedings of the 18th World Conference on Earthquake Engineering, WCEE2024, Milan, Italy, https://proceedings-wcee.org/.

Martí Molist, J. (2017). Assessing Volcanic Hazard: A Review. Oxford Handbook Topics in Physical Sciences, Oxford Academic, doi:10.1093/oxfordhb/9780190699420.013.32.

Marzocchi, W., J. Selva and T. H. Jordan (2021). A unified probabilistic framework for volcanic hazard and eruption forecasting, Nat. Hazards Earth Syst. Sci., 21, 11, 3509-3517, doi:10.5194/nhess-21-3509-2021.

Mastin, L. G., M. J. Randall, H. F. Schwaiger and R. P. Denlinger (2013). User's guide and reference to Ash3d – A three-dimensional model for Eulerian atmospheric tephra transport and deposition, Open-File Report, Reston, VA, 25, http://pubs.er.usgs.gov/publication/ofr20131122.

Meletti, C., W. Marzocchi, V. D'Amico, G. Lanzano et al. (2021). The new Italian Seismic Hazard Model (MPS19), Ann. Geophys., 64, 1, SE112, 2021, doi:10.4401/ag-8579.

Meredith, E. S., S. F. Jenkins, J. L. Hayes, N. I. Deligne et al. (2022). Damage assessment for the 2018 lower East Rift Zone lava flows of Kīlauea volcano, Hawaii, Bull. Volcanol., 84, 7, 65, doi:10.1007/s00445-022-01568-2.

Mossoux, S., M. Saey, S. Bartolini, S. Poppe et al. (2016). Q-LAVHA: A flexible GIS plugin to simulate lava flows, Comput. and Geosci., 97, 98-109, doi:10.1016/j.cageo.2016.09.003.

Pagani, M., D. Monelli, G. Weatherill, L. Danciu et al. (2014). OpenQuake engine: An open hazard (and risk) software for the global earthquake model, Seismol. Res. Lett., 85, 3, 692-702, doi:10.1785/0220130087.

Patra, A. K., A. C. Bauer, C. C. Nichita, E. B. Pitman et al. (2005). Parallel Adaptive Numerical Simulation of Dry Avalanches Over Natural Terrain, J. Volcanol. Geophys. Res., V139, 1-21, doi:10.1016/j.jvolgeores.2004.06.014.

Pomonis, A., R. Spence and P. Baxter (1999). Risk assessment of residential buildings for an eruption of Furnas volcano, São Miguel, the Azores, J. Volcanol. Geotherm. Res., 92, 107-131, doi:10.1016/S0377-0273(99)00071-2.

Schilling, S. P. (2014). LaharZ_py: GIS Tools for Automated Mapping of Lahar Inundation Hazard Zones, in Open-File Report 2014-1073, U. S. Geological Survey, Reston, Virginia, United States, 78, https://pubs.usgs.gov/of/2014/1073.

Schwaiger, H. F., R. P. Denlinger and L. G. Mastin (2012). Ash3d: A finite-volume, conservative numerical model for ash transport and tephra deposition, J. Geophys. Res., AGU, V117, B4, doi:10.1029/2011JB008968.

Servicio Geológico Colombiano, SGC (2015). Mapa de amenaza del volcán Nevado del Ruiz, tercera versión 2015. Escala 1:120.000. Servicio Geológico Colombiano, Observatorio Vulcanológico y Sismológico de Manizales, https://www2.sgc.gov.co/sgc/volcanes/VolcanNevadoRuiz/Documents/Mapa_de_Amenaza-VNR_v3-2015.pdf.

Silva, V., H. Crowley, M. Pagani and D. Monelli (2014). Development of the OpenQuake engine, the Global Earthquake Model's open-source software for seismic risk assessment, Nat. Hazards, 72, 3, 1409-1427, doi:10.1007/s11069-013-0618-x.

Silva, V., D. Amo-Oduro, A. Calderon, C. Costa et al. (2020). Development of a global seismic risk model, Earth. Spectra, 36, 1 suppl., 372-394, doi:10.1177/8755293019899953.

Spence, R., I. Kelman, P. Baxter, G. Zuccaro et al. (2005). Residential building and occupant vulnerability to tephra fall, Nat. Haz. Earth Syst. Sci., 5, 477-494, doi:10.5194/nhess-5-477-2005.

Torres-Corredor, R. A., P. Ponce-Villarreal and D. M. Gómez-Martínez (2017). Vulnerabilidad física de cubiertas de edificaciones de uso de ocupación normal ante caídas de ceniza en la zona de influencia del volcán Galeras, Bol. Geol., 39, 2, 67-82, doi:10.18273/revbol.v39n2-2017005.

Wild, A. J., J. M. Lindsay, M. S. Bebbington, M. A. Thompson Clive et al. (2020). Suitability of quantitative volcanic hazard and risk assessment methods and tools for crisis management in Auckland, New Zealand, Lower Hutt, GNS Science Report, 34, doi:10.21420/NGM3-5R75.

Yepes-Estrada, C., V. Silva, T. Rossetto, H. Crowley et al. (2016). The Global Earthquake Model Physical Vulnerability Database, Earthq. Spectra, 32, 4, 2567-2585, doi:10.1193/011816EQS015DP.

Yepes-Estrada, C., A. Calderon, C. Costa, H. Crowley et al. (2023). Global building exposure model for earthquake risk assessment, Earthq. Spectra, 39, 4, 2212-2235, doi:10.1177/87552930231194048.

Zuccaro, G., F. Cacace, R. Spence and P. Baxter (2008). Impact of explosive eruption scenarios at Vesuvius, J. Volcanol. Geotherm. Res., 178, 416-453, doi:10.1016/j.jvolgeores.2008.01.005.

***CORRESPONDING AUTHOR: Catalina YEPES-ESTRADA**,
Global Earthquake Model (GEM) Foundation, Pavia, Italy
e-mail: catalina.yespes@globalquakemodel.org